Application of a near coincidence site lattice theory to the orientations of $La_{2/3}Sr_{1/3}MnO_3$ grains on (001) $LaAlO_3$

1997 J. Phys.: Condens. Matter 9 7855

(http://iopscience.iop.org/0953-8984/9/37/016)

J. Phys.: Condens. Matter **9** (1997) 7855–7860. Printed in the UK PII: S0953-8984(97)82736-1

Application of a near coincidence site lattice theory to the orientations of $La_{2/3}Sr_{1/3}MnO_3$ grains on (001) $LaAlO_3$

Lei Shi†, Jie Gao†, Guien Zhou† and Yuheng Zhang†‡

† Structure Research Laboratory, University of Science and Technology of China, Hefei, Anhui 230026, People's Republic of China

‡ CCAST, World Laboratory, Beijing 100080, People's Republic of China

Received 18 March 1997, in final form 28 May 1997

Abstract. Various orientations of $La_{2/3}Sr_{1/3}MnO_3$ grains in polycrystalline films prepared on (001) $LaAlO_3$ substrates by the d.c. sputtering method were studied by x-ray diffraction experiments. The relation between the *a* and *b* axes of the $La_{2/3}Sr_{1/3}MnO_3$ thin film and the in-plane lattice vectors of the $LaAlO_3$ substrate has been directly obtained by an x-ray reflection β scan. The orientational relations agree well with the predication of a simplified theory of a near-coincidence site lattice between $La_{2/3}Sr_{1/3}MnO_3$ and $LaAlO_3$. The $La_{2/3}Sr_{1/3}MnO_3$ grains were found to have a high probability of forming low-angle or low-Σ boundaries among themselves. These grain boundaries are of low energy, free from extraneous phases, and exhibit a high connectivity of Mn–O–Mn nets. Therefore, the boundaries can still support the GMR effect.

A huge negative magnetoresistance observed near room temperature [1, 2] and the structural phase transition induced by an external magnetic field [3] in the perovskite Mn oxides $La_{1-x}D_xMnO_3$ with D = Ca, Sr, Ba have been subjects of very intensive experimental and theoretical studies for the last few years. Although heteroepitaxial films contain a high density of dislocations and strain due to a large difference in lattice constants and thermal expansion coefficients, heteroepitaxial growth was widely investigated using $NdGaO_3$, MgO, $SrTiO_3$ and $LaAlO_3$ as substrates [4–7]. $La_{1-x}D_xMnO_3$ is usually grown by molecular beam epitaxy (MBE), pulsed laser deposition (PLD) and the d.c. sputtering method. Microstructure of $La_{2/3}Sr_{1/3}MnO_3$ films on (001) $LaAlO_3$ substrates has been studied by several groups. It is possible to obtain films with the *c* axis of most of the grains normal to the substrate. However, the *a* and *b* axes of the $La_{2/3}Sr_{1/3}MnO_3$ grains are locked into several different orientations with respect to the $LaAlO_3$ axes, the most common ones being [100] $La_{2/3}Sr_{1/3}MnO_3$‖[100] $LaAlO_3$ and [110] $La_{2/3}Sr_{1/3}MnO_3$‖[100] $LaAlO_3$. In spite of their polycrystalline nature, these films can exhibit a decent giant magnetoresistance (GMR) effect. Recently, a thousandfold decrease in resistance was obtained in an epitaxially grown film of La–Ca–Mn–O which was post-annealed to obtain the highest magnetoresistance value [8, 9]. Polycrystalline films of the same composition, on the other hand, gave magnetoresistance ratios of only several hundred per cent. The actual behaviour depends on the sample composition and preparation process. In particular, the as-deposited films require special postannealing procedures in order to achieve a higher GMR effect, sharper transition, and higher transition temperature. The experimental results [1, 9, 10] indicate that the grain boundaries deteriorate the GMR properties, in agreement

0953-8984/97/377855+06$19.50

with the observations that the bulk (polycrystalline) materials and nonepitaxial films do not have an impressive GMR effect [9]. Therefore, a good film quality appears to be the most important factor for a GMR effect. It is necessary to use a method to judge the film quality by the lattice relationship of the film and the substrate.

In this paper, we report on the result of a detailed search of all possible orientational relations between the $La_{2/3}Sr_{1/3}MnO_3$ grains and the $LaAlO_3$ substrate. We found that all the observed orientational relations match well with the predication of a simplified theory of a near-coincidence site lattice (NCSL) [11] for low-energy interfacial configurations between perovskite oxide $La_{2/3}Sr_{1/3}MnO_3$ and $LaAlO_3$ substrate. The $La_{2/3}Sr_{1/3}MnO_3$ grains, locked into the preferred orientations with respect to the substrate, have a high probability of forming special low-energy boundaries among themselves. These special boundaries are free from extraneous phases, and do not affect the transport and magnetic properties of the film.

The perovskite oxide $La_{2/3}Sr_{1/3}MnO_3$ thin films on (001) $LaAlO_3$ substrate used in this study were prepared by the d.c. sputtering method. During sputtering, a substrate temperature $T_s = 745\,^{\circ}C$ and base pressure 4.5×10^{-7} Torr were used. The sputtering pressure and time were 3×10^{-2} Torr and 2 h, respectively. The sputtering gases were O_2 and Ar with a ratio of 1:3. The sputtering power was 220 V (d.c.)/300 mA. The thickness of the film is about 600 nm. The resistance of the films was checked by using a standard four-probe technique with applied magnetic field up to 0.8 T, which exhibited a decent GMR effect. The largest $\delta\rho/\rho = [\rho(H) - \rho(0)]/\rho(0)$ is greater than 25% under the applied magnetic field of 0.8 T. The detailed results will be published elsewhere.

A rotating anode x-ray powder diffractometer with graphite monochromatized Cu Kα radiation and height-pulse analyser, type D/max-rA, was used for the measurements of (001) reflections in Bragg–Bentano (BB) geometry and rocking curves. The pole figures were obtained by the pole figure diffractometer using a special sample holder with both vertical and horizontal slits. The experimental Schultz geometry is depicted in figure 1. The gonimeter is set at the Bragg angle corresponding to the crystallographic plane of interest. The intensity distribution is then measured while rotating the sample simultaneously around α and β.

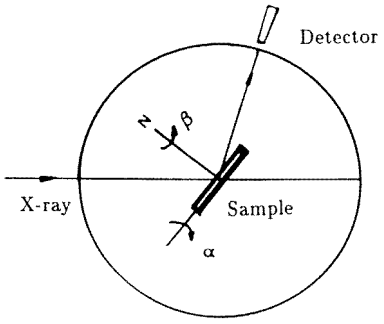

Figure 1. The experimental Schultz geometry showing the Bragg angle θ, the interface normal β and the tilt axis α.

The x-ray diffraction (XRD) pattern of an $La_{2/3}Sr_{1/3}MnO_3$ film in BB geometry is shown in figure 2. In BB geometry, the detector at 2θ received only the x-ray beam diffracted by the lattice planes at θ. It is found that the (001) diffraction peak of $La_{2/3}Sr_{1/3}MnO_3$ film and $LaAlO_3$ substrate are the diffraction patterns, while (001) planes of the substrate

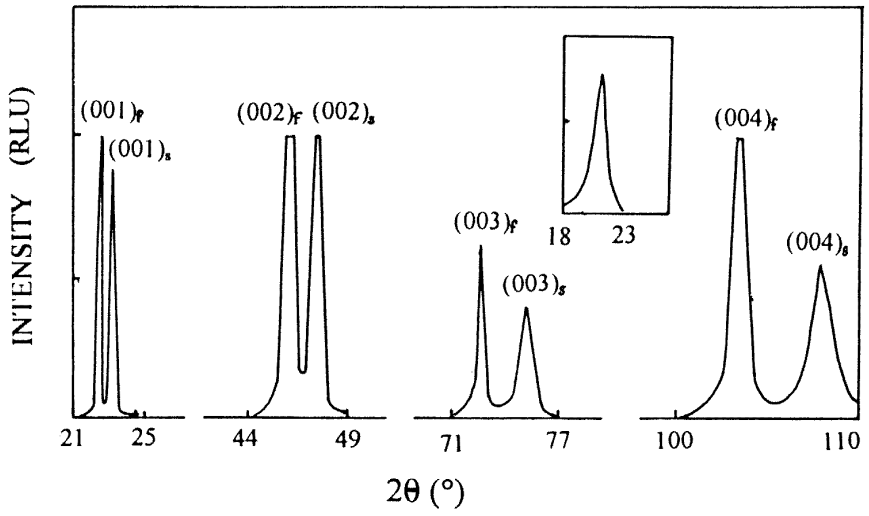

Figure 2. An XRD pattern in the BB geometry. Inset, x-ray θ-scan rocking curve of the (002) reflection of the film at fixed angle. s, substrate; f, film.

are parallel to the surface of the substrate, which confirms the epitaxial relationship (001) $La_{2/3}Sr_{1/3}MnO_3 \| (001)$ $LaAlO_3$. In order to establish a relation between the a and b axes of the c-axis-oriented $La_{2/3}Sr_{1/3}MnO_3$ film and the in-plane lattice vectors of the $LaAlO_3$ substrate, the {012} pole figure of the $La_{2/3}Sr_{1/3}MnO_3$ film and the {012} pole figure of the $LaAlO_3$ substrate were obtained by the pole figure diffractometer. The α and β rotations were coupled so that a 360° rotation of β corresponds to a 1° increase of α. The typical resulting pole figure using a polar stereognomonic net is presented in figure 3. (In figure 3, to show up the lattice symmetry we only give the main reflections. In fact, we also observed some very weak peaks appearing in the β scan of the (012) diffraction of the film, as shown in figure 4. These weak peaks give more information about the orientational relations between the c-axis-oriented $La_{2/3}Sr_{1/3}MnO_3$ film and the in-plane lattice vectors of the $LaAlO_3$ substrate.) Figure 3 shows the existence of fourfold symmetry in the in-plane lattice of the film. We note that a perfect crystal would show fourfold symmetry for both $\{012\}_{La_{2/3}Sr_{1/3}MnO_3}$ and $\{012\}_{LaAlO_3}$, rotated with respect to each other by 90° around the interface normal. From figure 4, it can be obtained that the [012] of $La_{2/3}Sr_{1/3}MnO_3$ is at several β angles to the [012] of the substrate, which suggests that the a and b axes of the $La_{2/3}Sr_{1/3}MnO_3$ grains are locked into several different orientations with respect to the $LaAlO_3$ axes. The observed and reported relative misorientation angles θ, the angles between $[100]_{La_{2/3}Sr_{1/3}MnO_3}$ and $[100]_{LaAlO_3}$, were compared to the theoretical predictions listed in the last column of table 1. Note that, due to the fourfold rotational and mirror symmetries of the film and substrate, all the misorientation angles are reduced to the range $0° \leqslant \theta \leqslant 45°$.

The coincidence site lattice (CSL) theory has been used to describe the formation of high-angle low-energy grain boundaries. Considering two interpenetrating crystal lattices, there exist some special misorientations which result in high densities of coincident lattice sites. The ratio of the crystal lattice sites to the coincident lattice sites is denoted by Σ. Since the lattice constants of $La_{2/3}Sr_{1/3}MnO_3$ are incommensurate to those of $LaAlO_3$, we use the NCSL theory to look for the interfacial configuration with a high density of near-

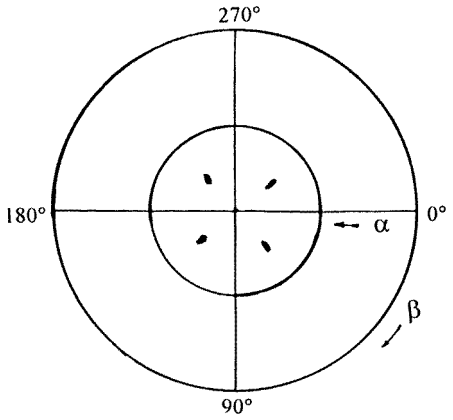

Figure 3. An XRD pole figure using a polar stereognomonic net of an $La_{2/3}Sr_{1/3}MnO_3$ film with $2\theta = 52.08^\circ$ (to show up the lattice symmetry, only the main reflections are given).

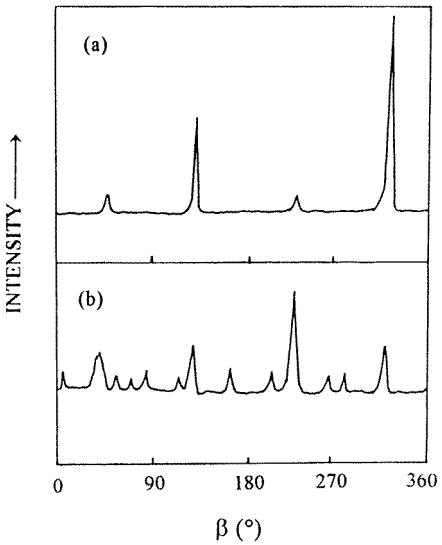

Figure 4. The β scan of (102) and (012) diffraction of (a) the substrate and (b) the film.

coincidence sites. Given the fact that the c axis of $La_{2/3}Sr_{1/3}MnO_3$ is always normal to the $LaAlO_3(001)$ surface, we only need to use a simplified two-dimensional version of the NCSL theory. Consider the $LaAlO_3$ surface as a square lattice for $LaAlO_3$ can be written as $\boldsymbol{T}_{LaAlO_3} = k\boldsymbol{a}_1 + l\boldsymbol{a}_2$ with the lengths given by $a\sqrt{\sigma_{LaAlO_3}}$ where $\sigma_{LaAlO_3} = k^2 + l^2$. σ, instead of Σ, is used here to denote two-dimensional coincidence. As discussed before, we treat the in-plane structure of $La_{2/3}Sr_{1/3}MnO_3$ also as a square lattice. The lattice constant b, unit vectors $\boldsymbol{b}_1$ and $\boldsymbol{b}_2$, translation vectors $\boldsymbol{T}_{La_{2/3}Sr_{1/3}MnO_3} = m\boldsymbol{b}_1 + n\boldsymbol{b}_2$, and $\sigma_{La_{2/3}Sr_{1/3}MnO_3} = m^2 + n^2$ are similarly defined for $La_{2/3}Sr_{1/3}MnO_3$. The degree of coincidence of these two square lattices is measured by the percentage misfit $\delta = 2(a\sqrt{\sigma_{LaAlO_3}} - b\sqrt{\sigma_{La_{2/3}Sr_{1/3}MnO_3}})/(a\sqrt{\sigma_{LaAlO_3}} + b\sqrt{\sigma_{La_{2/3}Sr_{1/3}MnO_3}})$. For a given NCSL, the angles between the coincident vector and the principal axes of $LaAlO_3$ and $La_{2/3}Sr_{1/3}MnO_3$

Table 1. Near-coincidence site lattices (NCSLs) for the [001] twist boundaries between $LaAlO_3$ and $La_{2/3}Sr_{1/3}MnO_3$ calculated with $\sigma_{LaAlO_3} \leqslant 35$ and $\delta < 2.5\%$ except for the case with $\sigma_{LaAlO_3} = 1$.

$LaAlO_3$			$La_{2/3}Sr_{1/3}MnO_3$				
H	K	σ_{LaAlO_3}	M	N	$\sigma_{La_{2/3}Sr_{1/3}MnO_3}$	δ (%)	θ (°)
1	0	1	1	0	1	3.50	0
3	0	9	2	2	8	2.39	45.0
3	1	10	3	0	9	1.77	18.4[a]
3	3	18	4	1	17	0.65	31.0[a]
4	1	17	4	0	16	0.47	14.0[a]
4	4	32	5	2	29	1.42	23.2[b]
5	1	26	4	3	25	1.54	25.6a[b], 41.8[a]
5	1	26	5	0	25	1.54	11.3[b]
5	2	29	5	1	26	1.96	10.5a[b], 33.1[a]

[a] Observed in this experiment.
[b] Not observed so far.

are given by $\tan^{-1}(l/k)$ and $\tan^{-1}(n/m)$, respectively. Hence, the relative misorientation angle between the $LaAlO_3$ and $La_{2/3}Sr_{1/3}MnO_3$ axes is $\theta = \tan^{-1}(l/k) \pm \tan^{-1}(n/m)$.

The smaller the misfit δ and the higher the density of near-coincidence sites (i.e., small σ_{LaAlO_3} and $\sigma_{La_{2/3}Sr_{1/3}MnO_3}$) are, the lower the interfacial energy is. We used a computer program to search for the NCSL and found that all the observed orientational relations can be matched by choosing $\sigma_{LaAlO_3} \leqslant 35$ and $\delta < 2.5\%$, except the $\theta = 0°$ case in which $\delta = 3.5\%$. The results are listed in table 1. Here we used $a = 0.3787$ nm and $b = 0.3922$ nm as the in-plane lattice constants for $LaAlO_3$ and $La_{2/3}Sr_{1/3}MnO_3$, respectively. Each of the observed misorientation angles is found to match one of the calculated values within the experimental error of $\pm 0.5°$. Also, all the calculated NCSLs with $\sigma_{LaAlO_3} \leqslant 35$ and $\delta < 2.5\%$ have been observed except the cases with $\theta = 10.5$, 11.3, 23.2 and 25.6°.

Having established that the $La_{2/3}Sr_{1/3}MnO_3$ grains and the $LaAlO_3$ substrate form several preferred [001] twist boundaries, we now consider the resulting [001] tilt boundaries between the $La_{2/3}Sr_{1/3}MnO_3$ grains. There are 14 distinct orientations observed for the $La_{2/3}Sr_{1/3}MnO_3$ grains as revealed in table 1 (counting $+\theta$ and $-\theta$ as different orientations except for $\theta = 0°$ and 45°). In principle, $14 \times 13 = 182$ types of inter-$La_{2/3}Sr_{1/3}MnO_3$-grain boundaries can be formed. Some of them are low-energy crystallographically special boundaries and some are of high energy. However, the high-energy grain boundaries may have a higher probability of being eliminated while the low-energy boundaries will develop into the dominant species.

It is difficult to control the exact stoichiometry of $La_{2/3}Sr_{1/3}MnO_3$ films. If the energy of an inter-$La_{2/3}Sr_{1/3}MnO_3$-grain boundary exceeds twice the interfacial energy between $La_{2/3}Sr_{1/3}MnO_3$ and an extraneous phase, impurities will diffuse to the boundary and form a dirty interface, which is catastrophic to the magnetoresistance. On the other hand, low angle and low-Σ boundaries are of low energy and they can remain microscopically clean.

Traditionally, all the physics controlling the basic properties of the systems was believed to be included in the 'double-exchange' model [12–14]. In the model, when hole doping is introduced, replacing 3+ valence ions with 2+ valence ions, the Mn^{3+}/Mn^{4+} ratio changes according to the doping level. It basically consists of the transfer of an electron between neighbouring Mn^{3+} and Mn^{4+} ions through the path Mn–O–Mn. This results in an effective ferromagnetic interaction due to the strong on-site Hund coupling. The two interactions,

one ferromagnetic and the other antiferromagnetic, compete to determine the magnetic structure. For $La_{2/3}Sr_{1/3}MnO_3$ grain boundaries on $LaAlO_3$ substrate, the low-angle and low-Σ boundaries are of low energy and thus free of extraneous phases. They should exhibit a significant fraction of connected Mn–O–Mn nets. For example, at a $\Sigma 9$ (300) boundary every other Mn–O–Mn chain is connected. These boundaries should still support the GMR effect. On the other hand, the existence of grain boundaries may change the orientational distribution of the Mn^{3+}/Mn^{4+} moment, which is an important factor for the existence of the GMR effect. The electronic and magnetic properties of the polycrystalline films are determined by the above two factors.

Acknowledgments

This project was supported by the Youth Science Foundation of the University of Science and Technology of China, and the National Natural Science Foundation of China.

References

[1] von Helmolt R, Weeker J, Holzapfel B, Schultz L and Samwer K 1993 *Phys. Rev. Lett.* **71** 2331
[2] Urushibara A, Moritomo Y, Arima T, Asamitsu A, Kido G and Tokura Y 1995 *Phys. Rev.* B **51** 14 103
[3] Asamitsu A, Moritomo Y, Tomika Y, Arlma T and Tokura Y 1995 *Nature* **373** 407
[4] Zeng X T and Wong H K 1995 *Appl. Phys. Lett.* **66** 3371
[5] Jakob G, Moshchalkov V V and Bruynseraede Y 1995 *Appl. Phys. Lett.* **66** 2564
[6] Achutharaman V S, Kraus P A, Vas'ko V A, Nordman C A and Goldman A M 1995 *Appl. Phys. Lett.* **67** 1019
[7] Xiong G C, Li Q, Ju H L, Greene R L and Venkatesan T 1995 *Appl. Phys. Lett.* **66** 1689
[8] Jin S, Tiefel T H, McCormack M, Fastnacht R A, Ramesh R and Chen L H 1994 *Science* **264** 413
[9] McCormack M, Jin S, Tiefel T H, Fleming R M, Phillips J M and Ramesh R 1994 *Appl. Phys. Lett.* **64** 3045
[10] Ju H L, Kwon C, Li Q, Greene R L and Venkatesan T 1994 *Appl. Phys. Lett.* **65** 2108
[11] Balluffi R W, Brokman A and King A H 1982 *Acta Metall.* **30** 1453
[12] Zener C 1951 *Phys. Rev.* **82** 403
[13] Anderson P W and Hasegawa H 1955 *Phys. Rev.* **100** 675
[14] de Gennes P-G 1960 *Phys. Rev.* **118** 141